Next Energy 7 (2025) 100291

Contents lists available at ScienceDirect

Next Energy

journal homepage: www.sciencedirect.com/journal/next-energy

Research article

Hazelnut shells and rice husks activated biochars for the adsorption of atrazine and terbuthylazine

Federico Apolloni[a,b], Federica Menegazzo[a,*], Carla Bittencourt[b], Michela Signoretto[a]

[a] CATMAT Lab, Department of Molecular Sciences and Nanosystems, Ca' Foscari University of Venice and INSTM-RU Ve, Via Torino 155, Venezia Mestre 30172, Italy
[b] ChIPS, University of Mons, Mons 7000, Belgium

ARTICLE INFO

Keywords:
Hazelnut shells biochars
Rice husk biochars
Activated biochar pyrolysis
Herbicides adsorption
Atrazine adsorption
Terbuthylazine adsorption
Waste biomasses
Biomass valorization

ABSTRACT

This study investigates the synthesis, characterization, and efficiency of activated biochars derived from second-generation biomasses—specifically hazelnut shells and rice husks—for remediating water contaminated with herbicides, including atrazine and terbuthylazine. These biomasses, recognized as agricultural wastes from high-yield crops, undergo a 2-step processing method: initial slow pyrolysis at 700 °C, followed by physical activation using steam at 850 °C. The resulting biochars, both in their natural and activated forms, were characterized using various analytical techniques, including elemental analysis, ash content determination, nitrogen physisorption, Fourier-transform infrared spectroscopy, and programmed temperature desorption. The adsorption capacity of the biochars was initially evaluated using trichloroethylene as a model molecule to simulate the adsorption mechanism of triazine herbicides. After determining the maximum adsorption capacity of the pollutant, adsorption tests for atrazine and terbuthylazine were conducted. The biochars adsorbed up to 93% of the 2 pollutants in the tests. These findings highlight the potential of activated biochars derived from second-generation waste biomass as an effective and sustainable alternative to conventional commercial activated carbons for purifying herbicide-contaminated water.

1. Introduction

Since the early 20th century, the industrial synthesis of ammonia has significantly increased the availability of synthetic fertilizers in agriculture. Simultaneously, the development and use of synthetic pesticides have surged over the past century, with global average pesticide consumption now reaching 1.58 kg per hectare per year [1]. Europe ranks third in pesticide consumption, using 505,000 tonnes in 2021, behind Asia (980,000 tonnes per year) and the Americas (1.12 million tonnes per year) [2]. The extensive use of pesticides increases the risk of their leaching into the soil after application, potentially contaminating groundwater and surface water bodies such as rivers and lakes.

Most pesticides in wastewater are organic, chemically stable, and non-biodegradable compounds. These substances are difficult to remove using conventional water and sewage treatment methods such as coagulation, filtration, or biological treatments. One effective solution for removing both organic and inorganic pollutants is adsorption. This method is favored for its high efficiency and the wide range of available sorbents, including activated carbons, zeolites, clay materials, and naturally derived sorbents [3]. Activated carbon is one of the most effective sorbents used in environmental protection. Its sorption capacity is primarily evaluated based on the analysis of its porous structure—including specific surface area, pore volume (micro-, meso-, and macropores), pore size, and distribution—as well as the chemical nature of its surface, particularly the presence of acidic and basic oxygen functional groups [4].

Since pesticide adsorption onto activated carbon is the most widely used method for water purification, a key aspect is the production of activated carbon itself. Today, there is a growing focus on more sustainable alternatives, such as agricultural by-products and residual waste. These by-products, primarily composed of shells, kernels, seeds, hulls, and husks, are commonly used as animal feed or as material for combustion and co-generation of energy [5]. Despite their potential applications, a significant portion of these by-products is discarded in disposal sites, posing an environmental challenge. These biomasses are valuable sources of cellulosic material, primarily composed of cellulose, hemicellulose, and lignin, with varying amounts of inorganic compounds depending on the original agricultural product. Such biomasses serve as promising raw materials for the development of activated

* Corresponding author.
E-mail address: federica.menegazzo@unive.it (F. Menegazzo).

https://doi.org/10.1016/j.nxener.2025.100291
Received 14 February 2025; Received in revised form 1 April 2025; Accepted 8 April 2025

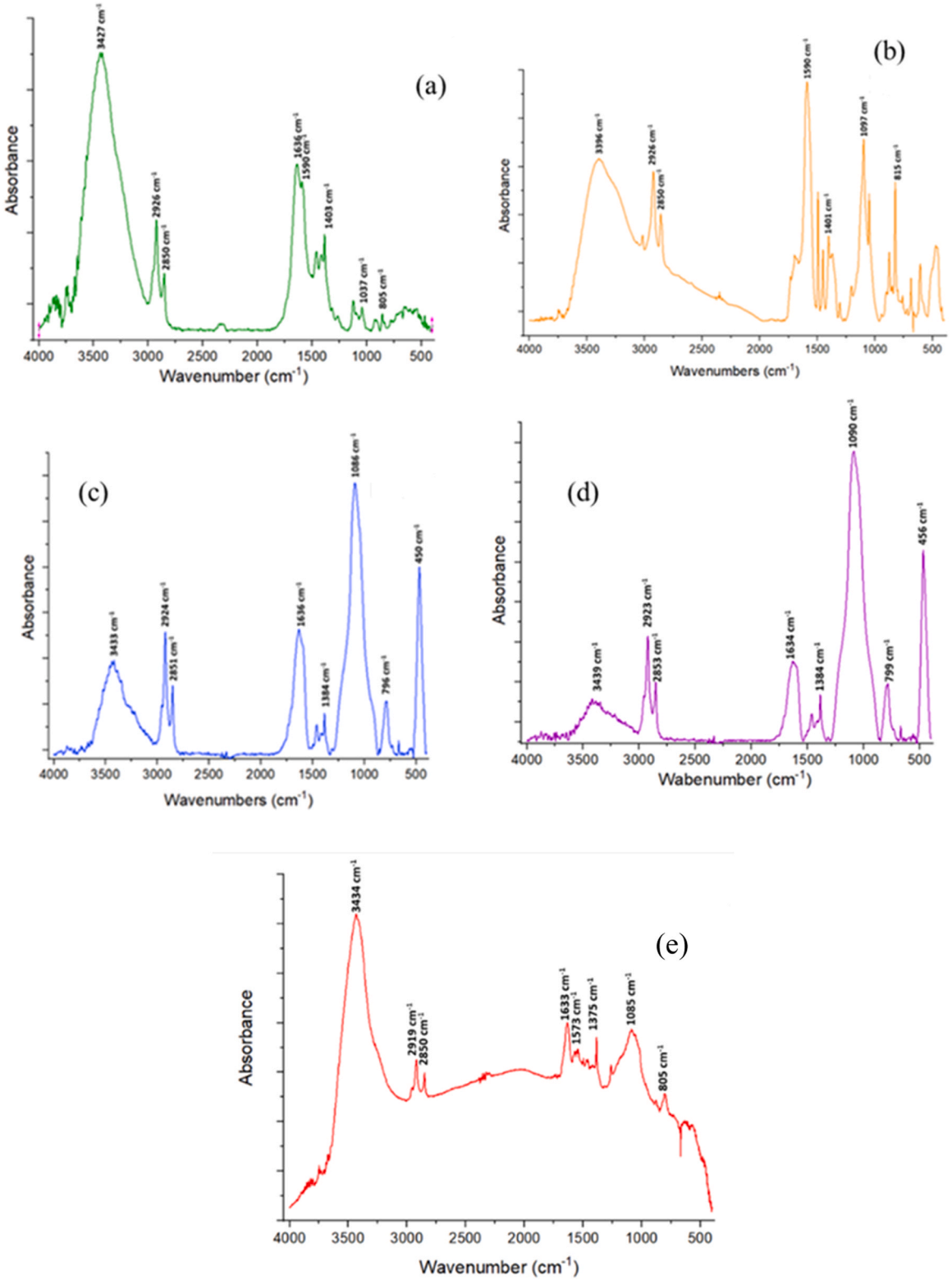

Fig. 1. FT-IR spectra of synthesized biochars, AH (a), H (b), AR (c), R (d) and the commercial activated carbon (e). FT-IR, Fourier-transform infrared spectroscopy.

biochars. In this study, rice husks and hazelnut shells, both second-generation biomasses. were selected as second-generation biomasses. Chemically, both are lignocellulosic materials composed of varying proportions of lignin, cellulose, and hemicellulose. Those 2 biomasses are of great availability in Italy. In fact, Italy stands as the seconds largest rice producer in the European Union [6], with China leading the world with 28% of the global production [7]; moreover, Italy is regarded as the second largest hazelnut producer in the world, right behind Turkey [8].

Among various pesticide classes, herbicides are crucial for weed management in agricultural crop areas. Among various pesticide classes, herbicides play a crucial role in weed management in agricultural crop areas. Atrazine, also known as 6-Chloro-N^2-ethyl-N^4-(propan-2-yl)-1,3,5-triazine-2,4-diamine, is a selective triazine

herbicide with root action, commonly used in pre- and post-emergence applications for crops such as corn, soy, and sugarcane. However, due to its persistence in water and the environmental risks it poses, atrazine has been banned in the EU since 2004 [9]. Terbuthylazine (TBA), chemically known as 2-N-tert-butyl-6-chloro-4-N-ethyl-1,3,5-triazine-2,4-diamine, replaced atrazine in the EU following its ban. Like atrazine, TBA is a systemic, root-absorbing herbicide used in pre- and post-emergence applications for soy and maize cultivation. Its persistence in the environment is primarily due to its low water solubility (33 mg/L at 25 °C) and its long half-life, which ranges from 79 to 203 days depending on various factors [10]. TBA has a half-life which varies from 76 to 331 days, depending on the matrix and light conditions [11]. Atrazine and terbuthylazine, despite being both a selective herbicide, are also a dangerous threat to aquatic fauna and flora, interfering with their survival, growth and reproduction [12,13]. Another problem related to the use of these 2 herbicides is their degradation products, which can be even more persistent and dangerous than the herbicide itself.

Both herbicides pose a potential threat to the water reserve of the European Union with illegal levels of TBA and atrazine have been detected in the hydrographic basins of rivers Adda and Oglio [14] as well as along the river Po [15] and various locations across Europe [16,17]. Moreover, even many years after the ban, dangerous concentrations of atrazine can be found in illegal concentrations underwater, soil and surface water [18]. This huge mass of contaminated water must be purified, and various methods are being developed. For example, atrazine and TBA can be treated and removed from the water with a TiO_2-based photocatalytic oxidation [19], or UV and UV/H_2O_2 photodegradation [20], biodegradation [21] or the adsorption of the pesticides on the activated carbon [22]. The last is considered the most promising method since it combines low operational and production cost, great availability on the planet and the ability to treat a larger quantity of water in comparison to the other mentioned methods. The adsorption of activated carbon shows a high removal efficiency and the absence of byproducts. The diffusion of these adsorbents is primarily related to their superior characteristics in terms of superficial area, porosity, functional groups, and superficial activities [23].

The main objective of this study was to develop activated biochars derived from waste biomasses and evaluate their adsorption properties for herbicides commonly found in wastewater. The activated carbons were produced through the pyrolysis of rice husks and hazelnut shells, followed by the physical activation of the resulting biochars. Pyrolysis is considered one of the most promising techniques for the thermal valorization of waste biomass and has become a focal point of extensive research within the scientific community. The unique aspect of this thermal process is its ability to produce a diverse range of products across all 3 phases (solid, liquid, and gas) from a single biomass source. The effectiveness of the biochars in herbicide removal was assessed in batch tests, using trichloroethylene as a model molecule and atrazine and TBA as target herbicides.

2. Methods and materials

Atrazine and terbuthylazine are of analytical grade (> 99.9%) and are acquired from Sigma-Aldrich. Methanol, Dichloromethane, Trichloroethylene, 1,2 Dichloroethane, Sodium Sulfate (Na_2SO_4), and Sodium Chloride (NaCl) are 99% pure and acquired from Sigma-Aldrich.

Hazelnut shells from cultivar Tonda Gentile Romana were kindly supplied by Fattoria Lucciano Soc. Agr. S.s., Civita Castellana, Viterbo, Italy. Rice husks were kindly supplied from Riseria delle Abbadesse, Grumolo delle Abbadesse, Vicenza, Italy.

A high-surface commercial activated carbon supplied by Acque Veronesi S.P.A. was used as a reference.

2.1. Pyrolysis and activation

The biomasses chosen for this work are Rice husk and Hazelnut shells. The Hazelnut shells were selected to have a mesh between 7 and 10, while the Rice husks were used as they are.

The pyrolysis was performed in a laboratory-scale prototype rig (Carbolite custom model EVT 12/450B), consisting of a vertical tubular oven in which a fixed-bed quartz tube can be inserted (Fig. 1). The temperature of the oven was controlled by a temperature controller Eurotherm 3508P1. Inside the quartz tube, usually 50 g of biomass was inserted, and the pyrolysis was conducted in a flow of N_2 of 100 mL/min for 30 min, with a target temperature of 700 °C and a temperature ramp of 5 °C/min.

After the pyrolysis, the biochars were activated in a prototype lab-scale activation plant. A small quantity of biochar, usually between 3 and 8 g, was inserted into a quartz tube. The biochar is brought to a temperature of 850 °C at a rate of 10 °C/min in the presence of a 50 vol % steam/N_2 mixture with a total gas flow of 100 mL/min. These conditions are maintained for 90 min. The hazelnut shells biochar is indicated as H, the physical activated hazelnut biochar as AH, the rice husk biochar as R and the physical activated rice husk biochar as AR.

2.2. Characterization of the biochars

The elemental composition of the samples is determined with the help of UNICUBE organic elemental analyser. Carbon is measured as CO_2, and hydrogen is measured as H_2O. The oxygen content can be calculated by difference according to Eq. (1).

$$O\% = 100 - (C\% + H\% + N\% + S\% + ash\%)$$

Equation 1. Determination of oxygen.

The ash content of the activated carbons was determined using the standard American Society for Testing and Materials D3174-00 method. The percentage of ash presented within each sample was determined by Eq. (2):

$$\%ash = [(A-B)/C] \text{ X } 100$$

Equation 2. Determination of ash percentage.

where:

A is the mass of the crucible with the ash, expressed in grams.

B is the mass of the crucible, expressed in grams.

C is the mass of the sample under analysis, expressed in grams.

The physisorption analyses were performed at −196 °C using the Tristar II Plus Micromeritics. The sample (≈0.04 g) was placed under vacuum using a vacuum degasser system of Micromeritics (VacPrep 061) at 0.15 mbar and previously treated at 200 °C for 2 h to eliminate moisture or any other contaminants that may be absorbed. The isotherm resulted from this adsorption and desorption were fitted according to the Langmuir or Brunauer–Emmett–Teller adsorption model.

The FTIR spectroscopy analysis were performed using the KBr tablet methodology with the tablets subjected to a pressure of 10 t/cm [2] and then analysed using a Perkin Elmer Precisely Spectrum IR spectrometer with a resolution of 4 cm^{-1} and an average of 256 scans.

The TPD (Temperature Programmed Desorption) measures were executed with the sample (150 mg) loaded into a fixed-bed, U-shaped quartz reactor inserted into an oven linked to a temperature programmer. The temperature was heated to 1000 °C with a heating rate of 10 °C/min (Eurotherm mod.8080) in helium flow. The effluent gases were monitored by a Gow-Mac thermal conductivity detector (TCD).

The elemental composition and chemical activation of the samples were evaluated using X-ray photoelectron spectroscopy (XPS) with a PHI Genesis instrument from Physical Electronics (Chanhassen, MN, USA), equipped with a monochromatic Al Kα X-ray source. To compensate for charge build-up during X-ray irradiation, a dual-mode charge compensation was used. The binding energy was calibrated

Table 1
Elemental composition and ash content

Sample	N [%]	C [%]	H [%]	S [%]	O [%]	Ash [%]	N + O [%]
H	0.31	86.07	2.25	0.12	9.43	1.78	9.74
R	0.44	50.91	1.23	0.22	2.36	44.48	2.80
AH	0.21	88.98	0.98	0.12	9.22	0.49	9.41
AR	0.17	38.63	0.44	0.12	4.01	56.63	4.18
Commercial	0.37	87.11	0.69	0.49	1.34	10.0	1.71

based on the C 1 s peak at 284.6 eV.

2.3. Adsorption test

2.3.1. Trichloroethylene adsorption test

Around 50 mg of activated carbon, previously washed for 48 h in distilled H_2O, were filtered and inserted into a vial with 1 mL of a previously prepared solution of 25,000 ppm of trichloroethylene in methanol and 4 mL of distilled water. The vials were inserted into a tilting plate at 180 rpm and analysed after 30, 60, 120, 180, 360, and 1440 min. For the analyses, 2 mL of the solution was withdrawn from the vial using a syringe, filtered, and poured into an assay tube. Then, internal standard (1,2-dichloroethane), 7.2 mL of dichloromethane, and 300 mg of NaCl were added. The tube was mixed for 15 s on the vortex and for 3 min in the spin cycle at 6000 rpm. Using a syringe, the organic phase was withdrawn from the tube, and 300 mg of Na_2SO_4 was added. The analyses were performed with a gas chromatograph (Agilent 7820 A) equipped with an Agilent HP-5 column and an flame ionization detector.

2.3.2. Atrazine and terbuthylazine adsorption test

Around 50 mg of activated carbon, previously washed for 48 h in distilled H_2O, were filtered and inserted into a 100 mL flask. Then, 3.1 mL of a previously prepared 1000 ppm solution of atrazine and terbuthylazine in methanol and 27,9 mL of milliQ water were added. The flask was inserted in a batch-type reactor to simulate a water depuration plant for 60 min at 25 °C. Samples were taken every 5 min. The analyses were conducted using an Agilent Technologies 1260 Infinity II High-performance liquid chromatography equipped with a C18 Column and VW detector.

3. Results and discussion

3.1. Preliminary characterization of the biochars

In this study, the activated carbons were produced through the pyrolysis of rice husks and hazelnut shells, followed by the subsequent physical activation of the biochars. According to previous studies, the main factors regulating the adsorption of atrazine and terbuthylazine onto the activated biochar include the starting biomass [24], the temperature, the pyrolysis type [25] and the adsorption mechanism [26]. The adsorption capacity of activated carbon depends on several factors, including its pore structure, surface area, surface chemistry, and the specific properties of the molecules being adsorbed, such as their size, structure, and polarity [27]. Pyrolysis temperature is the primary factor influencing the properties of biochar [28]. It is important to note that biochars produced at high temperatures typically have low O/C and H/C ratios, are predominantly composed of aromatic carbon, and exhibit a large surface area and high microporosity [29]. To further enhance the porosity and surface properties of biochars, an activation process is required. Two common activation methods are chemical activation and physical activation. Chemical activation involves the use of a chemical activating agent, such as zinc chloride ($ZnCl_2$), potassium hydroxide (KOH), or phosphoric acid (H_3PO_4). Due to the hazardous nature of these activating agents, a washing step is necessary to remove the impregnating agent [30]. The other method, physical activation, is considered more sustainable as it only requires electricity (which can be sourced from renewable energy) and steam or CO_2 as the activating agent. This process involves exposing the biochar to a controlled gas stream at temperatures between 700 and 950 °C. Common activating gases include CO_2, aqueous steam, or a mixture of the 2. Notably, a controlled steam flow has higher oxidizing power, greater reactivity with biochar, and is more efficient at increasing the biochar's surface area than CO_2 [31]. The combination of high temperature and steam exposure opens closed pores on the biochar surface, leading to increased surface area and porosity [32]. The key parameters for physical activation are the time of exposure and temperature—higher values result in greater increases in surface area and porosity [33]. The biochars, in both their natural and activated states, were characterized using various techniques such as elemental analysis and ash content, nitrogen physisorption, FTIR spectroscopy, TPD and XPS. These techniques were employed to study the physical-chemical, morphological, and structural properties of the different activated biochars, along with a commercial activated carbon, which served as a reference.

The first measurements were elemental analyses, as reported in Table 1.

Samples AH and H exhibit a very high carbon content, as they originate from lignocellulosic biomass with a high lignin content [34]. Such biomass typically facilitates the formation of activated biochars with high carbon content and a more homogeneous and orderly structure [35]. On the other hand, AR and R-activated biochars are characterized by a much lower carbon content since this char derives from lignocellulosic biomass with a high content of inorganic compounds, primarily composed of silica [36]. This data is confirmed by the ash content present within these samples, which reaches a value of about 57%, much higher than those observed for other carbon substrates. These results are consistent with the literature data since husks are typically composed of 70% organic compounds and 30% inorganic compounds such as silica [37], while the shells are made of around 40–50% lignin, with hemicellulose and cellulose percentages ranging between 13% and 32% and 16–27%, respectively with a small part of inorganic compounds [38,39].

As for the nitrogen physisorption analyses (Table 2), the commercial activated carbon, derived from mineral sources and physically activated, exhibits the highest surface area among all the samples analysed. AH is the second position for adsorption capacity while showing the highest contribution of microporous surface area. It is noteworthy that AR shows a lower surface area compared to AH, with only a slight

Table 2
Nitrogen physisorption analyses

Samples	S_{BET} (m^2/g)	$S_{Langmuir}$ (m^2/g)	V_{tot} (cm^3/g)	V_{micro} (cm^3/g)	V_{meso} (cm^3/g)
H	313	465	0.19	0.10	0.09
R	200	324	0.07	0.06	0.01
AH	637	1009	0.40	0.21	0.19
AR	357	609	0.28	0.10	0.18
Commercial	899	1400	0.57	0.17	0.40

S_{BET} = BET surface area; $S_{Langmuir}$ = Langmuir surface area; V_{tot} = total pore volume; V_{micro} = total micropore volume; V_{meso} = total mesopore volume.

increase in value compared to R. This difference can be explained by the high percentage of silica present in the rice husk sample, which remains unaltered by the activation treatment. In fact, the activating agent primarily interacts with the carbon atoms in the precursor, oxidizing them to CO and CO_2, thereby leading to the formation of pores [40], explaining the higher superficial area of the AH biochar compared to the AR one [41]. Indeed, there is a significant increase in the micropore area in AR compared to the non-activated rice husk biochar (R). This might be attributed to the steam activation. The presence of the CO originated from the oxidation of the carbon atom of the precursor can improve the surface area of biochar due to corrosion resulting in the improved microporous structure and increased pore volume [42]. This increase in the micropore surface area can partially justify the difference in adsorption capacity between the AR and the H biochar. Those results are comparable to the previous works found in literature, where the biochar investigated possesses a similar chemical composition [43] and superficial properties [44].

The curves resulting from the analysis of both the activated biochars (*AH* and *AR*) and the commercial activated carbon can be classified as hybrids between type I and type IV isotherms. These curves are indicative of materials characterized by the coexistence of micropores and mesopores. For low relative pressure values, there is a rapid and pronounced increase in the volume of gas adsorbed on the solid surface, typical of type I isotherms that characterize microporous systems. For higher partial pressures, the formation of hysteresis can be observed, a characteristic feature of type IV isotherms that characterize mesoporous systems. All the images of the physisorption curves can be found in the Supplementary Files.

On the other hand, the isotherms derived from non-activated biochars from rice husk and hazelnut shells (H and R) can be classified as type I isotherms, also known as Langmuir isotherms. These curves are typical of microporous materials, wherein rapid nitrogen adsorption on the surface occurs for low values of relative pressures, followed by a plateau phase where adsorption remains practically constant [45].

To investigate the nature of the functional groups, FTIR and TPD measurements were performed. As for FTIR analyses, the spectrum derived from the analysis of the AH, H, AR, AR biochars and the commercial activated carbon are shown in Fig. 1:

The spectra of the 2 hazelnut-derived biochars present many signals in common. The first one is located at 3427 cm^{-1} and 3396 cm^{-1} and is related to the stretching of -OH groups, probably derived from the presence those functional groups on the surface of the biochar. The 2 medium intensity bands located in the region between 2800 and 2900 cm^{-1} are attributed to the asymmetric (2926 cm^{-1}) and symmetrical (2850 cm^{-1}) stretching vibration of the C-H bond of the CH_2 group associated with aliphatic hydrocarbons. The signal detected in both spectra at 1590 cm^{-1} is reasonably associated with the C═C stretching vibration of aromatic systems [46]. The peak at 1403 and 1401 cm^{-1} is related to the C-H bending of an alkane group, indicating the presence of this type of functional group on the surface. The band centered at 1037, and 1097 cm^{-1} is associated with the stretching vibration of the C-O bond, while the 805 and 815 cm^{-1} bands are related to the stretching stretch of C-H present in aromatic systems [47]. The sharp peak at 1636 cm^{-1} can be attributed to the stretching vibration of C═O present in ketones, aldehydes, lactones or the carboxyl group and is the only signal that is characteristic of the AH biochar. The AR Fourier-transform infrared spectroscopy (FT-IR) spectrum shows 2 main differences in comparison with the AH biochar. The first is the attribution of the signal at 796 $cm^{-1,}$ which can also be attributed to the vibration of the Si-OH bond, typical of silica-based materials. The other is the presence of a peak in the fingerprint region at around 450 cm^{-1}, commonly associated with the stretching of the Si-O-Si bond of the SiO_2 present in this sample [48]. The FT-IR spectrum of the R biochar shows some peaks presented in the H spectra in the area between 4000 and 2000 cm^{-1}. After the 2000 cm^{-1}, some differences started to emerge. First is the presence of a strong peak at 1636 cm^{-1}, which can be attributed to the stretching vibration of C═O present in ketones and aldehydes, while the 1384 cm^{-1} band is related to the C-H bending of an alkane group, indicating the presence of this type of functional groups on the surface of the activated biochar. The band centered at 1090 cm^{-1} can be associated with the stretching vibration of the C-O bond. The bands detected at 799 and 456 cm^{-1} are visible only in the rice husk derived sample as they are associated respectively with the vibration of the Si-OH bond and with stretching of the Si-O-Si bond of SiO_2 present in this sample [49].

Looking at the commercial sample (d), the first signal considered is the stretching of the O-H bond of the OH groups located at 3434 cm^{-1}, probably originating from the hydroxyl groups present in the sample. The pair of peaks located respectively at 2850 and 2919 cm^{-1} can instead be attributed to the symmetrical and asymmetrical stretching of the C-H bonds of the terminal alkane groups located on the surface of the activated carbon. The strong peak at 1633 cm^{-1} stretching vibration of C═O present in ketones, aldehydes, lactones or the carboxyl group, while the signal detected at 1573 cm-1 originated from the stretching of C═C bonds of the aromatic compound presented on the commercial activated carbon. The peak at 1385 cm^{-1} is related to the C-H bending of an alkane group, indicating the presence of this type of functional group on the surface of the activated carbon. The broad signal located at about 1085 cm^{-1} can be attributed to the stretching of the C-O bond of the primary alcoholic groups of the activated carbon, while the peak detected at 805 cm^{-1} originated from the bending of the C-H bonds of poly-substituted alkenes.

TPD analysis has become a widespread technique for determining the oxygen-based functional groups present on the surface of carbonaceous materials [50]. In this type of analysis, the functional groups are thermally decomposed by releasing CO, CO_2, and H_2O at different temperatures depending on the thermal stability of the group being considered [51].

As for TPD analyses (Fig. 2), in the profile of the commercial sample, wide asymmetric bands are centered between 800 and 1000 °C, attributable to carbonyl and quinone groups, respectively, as well as bands in the range of 200–400 °C, reasonably due to the release of CO_2 from carboxyl groups and lactones. Broad peaks above 600 °C have been attributed to the release of CO and/or CO_2 from coal or other residues derived from the type of initial treatment the coal underwent and the porous structure.

In the TPD profiles of AH and H samples, there is a band at temperatures between 100 and 400 °C, associated with the CO_2 released by the decomposition of the carboxyl groups, and an additional band in the region between 600 and 800 °C, associated with the desorption of CO due to the thermal decomposition of ethers and phenols. Additionally, only for the AH sample, an additional band at over 800 °C is observed, associated with the generation of CO due to the thermal decomposition of quinones.

As for the AR and the R samples, both TPD profiles show a weak band in the region of 200–400 °C, indicating the presence of carboxyl groups, revealed by the release of CO_2 detected by the analysis. The other notable band shared by the 2 biochars is the one located at 600 °C, which can be attributed to the desorption of CO by the phenolic group on the surface of the biochar. The AR-activated biochar presents a signal at around 950 °C, too, probably originating from the release of CO from the quinone groups located on the activated carbon. The low intensity of the signal of these 2 samples can be attributed to the presence of ash on the activated carbon.

The results obtained from the elemental analysis, FT-IR, and TPD suggest that the different biochars examined have different surface functional groups due to the nature of the different biomasses from which they are obtained.

To better understand the properties of the commercial activated carbon and the AH biochar, they were characterized using XPS. This technique allows us to understand the nature and quantity of the functional groups present on the surface of the activated carbon. Figs. 3

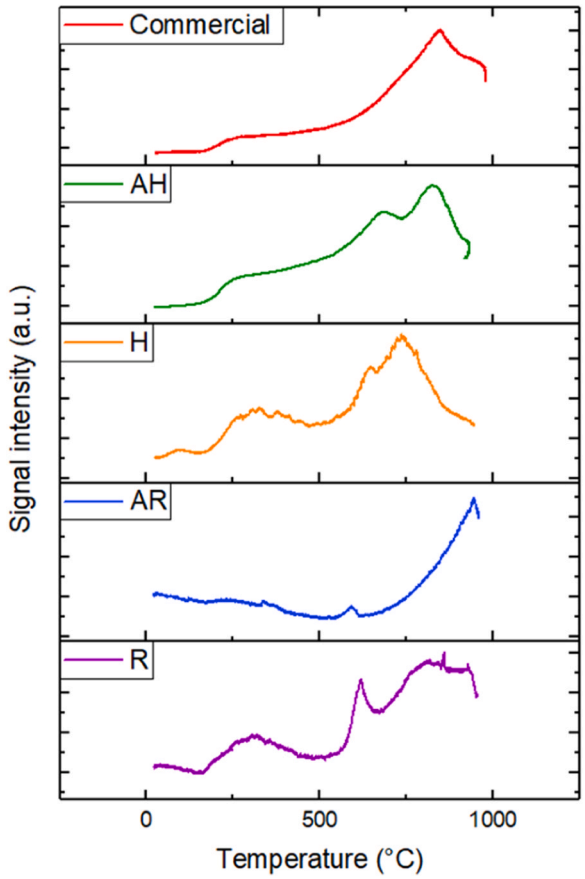

Fig. 2. TPD plots. TPD = temperature programmed desorption.

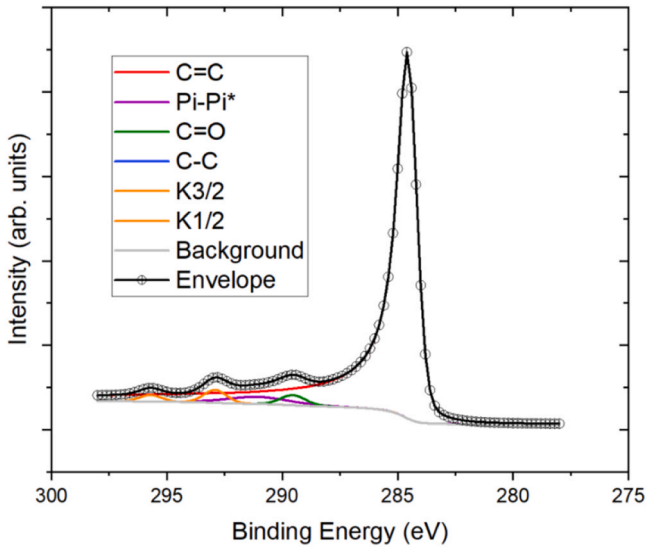

Fig. 3. C1s XPS analysis of the AH biochar. XPS = X-ray photoelectron spectroscopy.

and 4 show the XPS data collected for those 2 activated carbons.

For the analysis of the C1s XPS recorded on the AH-activated biochar, 4 singlets and 1 doublet were used. The analysis suggests a high graphitized phase due to the excellent agreement of the asymmetric component used to reproduce with the instrument signal, with the C=C peak centered at 284.5 eV with the experimental data and the presence of loss structure centered 291,2 eV due to plasmon interaction (π-π* interaction). The component centered at 289.4 eV indicates the presence of C=O groups. The presence of traces of K in the sample is

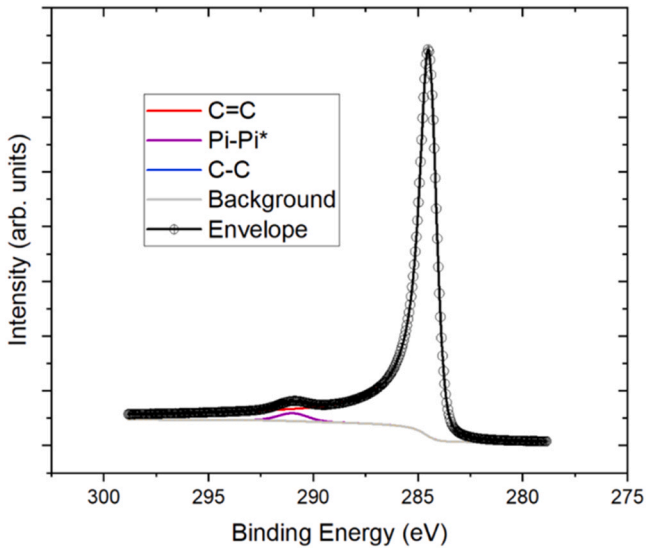

Fig. 4. C1s XPS analysis of the commercial activated carbon. XPS = X-ray photoelectron spectroscopy.

indicated by the K 2p doublet peak with components centered at around 292.8 eV (K $2p_{3/2}$) and 295.8 eV (K $2p_{1/2}$).

For the analysis of the C1s XPS recorded on the commercial sample, 2 singlets were used. The analysis suggests a high graphitized phase due to the excellent agreement of the asymmetric component used to reproduce the C=C peak centered at 284.5 eV with the experimental data and the presence of loss structure centered at 291.1 eV due to plasmon interaction (π-π* interaction).

3.2. Adsorption tests

The use of biochar derived from the pyrolysis of second-generation biomasses for the removal of atrazine and TBA is a relatively new and effective method for wastewater purification worldwide. Moreover, this process can be adapted to utilize biomass available near the contamination site, helping manage waste biomasses within the local country or region. For safety and cost reasons, trichloroethylene, a model molecule, was initially used, as it closely replicates the adsorption mechanism of triazine herbicides. Trichloroethylene has a water-octanol partition coefficient similar to that of atrazine and TBA, indicating a potential risk of bioaccumulation. Additionally, all 3 compounds have low solubility in water [52–54]. Moreover, this molecule shares similarities in the adsorption mechanism onto activated carbon, which is primarily influenced by the carbon content, the presence of C=C bonds on the activated biochar surface, as well as the biochar's high surface area and specific porosity. For herbicides, the interaction occurs between the π-electrons of the C=C bonds on the activated biochar surface and the π-electrons in the aromatic heterocyclic rings of the herbicides [55] while the trichloroethylene has C=C its double bonds interacting with the π-electrons on the surface of the biochar [56].

Fig. 5 shows the different interactions between the herbicides and the activated biochar surface.

These tests allowed us to determine the adsorption capacity of activated carbon, which can be defined as its ability to attract, capture, and retain gas or liquid molecules on the surface through the process of adsorption. As illustrated in Fig. 6, considering the biochars and activated biochars obtained from wastes, AH exhibits the highest adsorption capacity, with approximately 405 mg of pollutant adsorbed per milligram of activated biochar. AR follows as the second-best performer within the group, boasting an adsorption capacity that can reach around 329 mg/g. Conversely, the 2 non-activated biochars, R and H, demonstrate the lowest adsorption capacities, estimated at

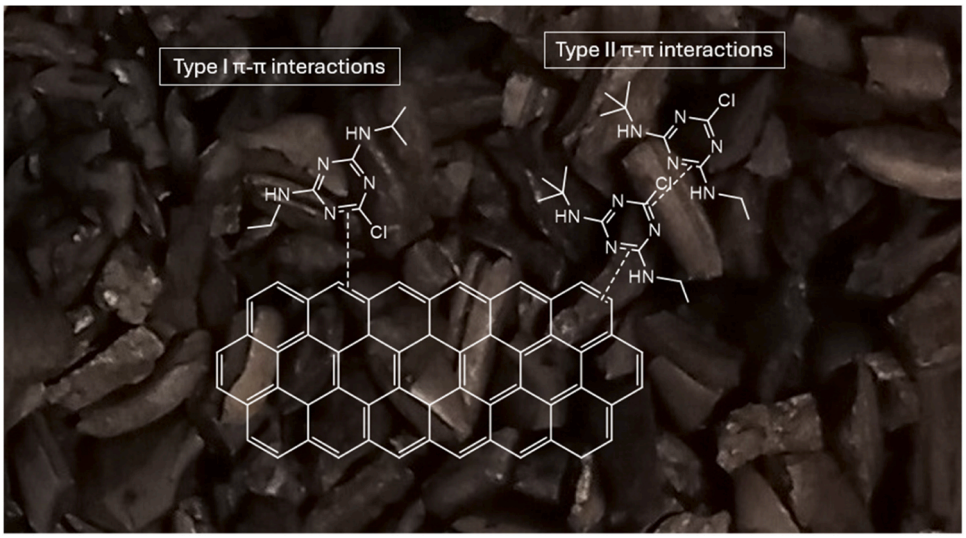

Fig. 5. Possible π-π interactions between the herbicides and the activated biochar.

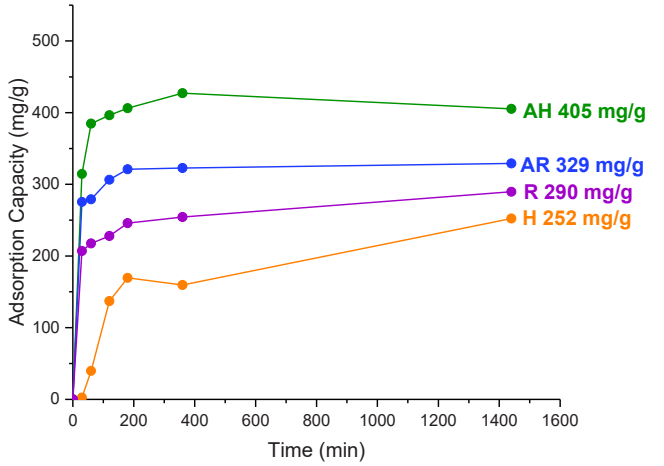

Fig. 6. Kinetics of trichloroethylene adsorption over 24 h on steam-activated hazelnut shells biochar (AH), hazelnut shells biochar (H), steam-activated rice husk biochar (AR), and rice husk biochar (R).

approximately 290 and 252 mg/g, respectively.

As evident from the graph in Fig. 6, the data obtained during the adsorption tests vary significantly from biochar to biochar in terms of adsorption capacity. Considering that the superficial area and the porosity are the most important parameter that influences the adsorption of the trichloroethylene onto the activated biochar, the primary disparities lie between the values reported for non-activated and activated biochar, as well as between the 2 different types of biochar derived from hazelnut shells and rice husk. These differences indicate that the performance of the biochars is strongly influenced by the activation process and the type of biomass used for pyrolysis. The starting biomass and the activation process are fundamental parameters that significantly determine the performance, chemical-physical, structural, and morphological properties of an activated carbon [57]. During the activation, the combination of high temperature and steam exposure opens closed pores on the biochar surface, leading to increased surface area and porosity, and the characterizations confirm that [58]. As seen by the test, the activated ones perform better than the non-activated ones.

The AH-activated biochar emerged as the best option. It was tested to determine the adsorption of atrazine and terbuthylazine, with the commercial activated carbon used as a comparison.

The starting concentration for the 2 herbicides in these tests is 100 ppm. According to the literature, the concentration of the 2 triazine molecules in ground and surface water rarely exceeds the 2.0-ppm value and is commonly assessed around 0.1 ppm. Additionally, the United States Environmental Protection Agency's (USEPA) Drinking Water Levels of Comparison (DWLOC), which represents the maximum concentrations in drinking water that, when considered together with dietary exposure, do not exceed a level of concern, range from 12.5 to 68 ppm for intermediate (seasonal) or chronic (annual) exposure [59]. Based on these assumptions, this starting concentration is considered adequate to replicate a year of water treatment in a depuration plant. Fig. 7 illustrates the variation of the concentration of the triazinic

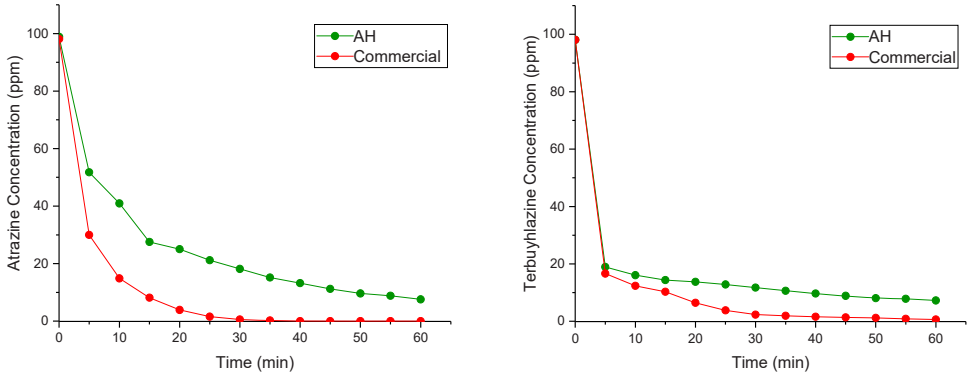

Fig. 7. Variation of the concentration of atrazine (left) and terbuthylazine (TBA, right) in the aqueous solution over 60 min onto commercial activated carbon, steam-activated hazelnut shells biochar (AH).

herbicides atrazine and terbuthylazine obtained from the tests conducted for the commercial activated carbon and the AH hazelnut shell activated biochar. The data is presented in terms of ppm of atrazine and terbuthylazine adsorbed by the carbonaceous system over one hour of reaction time.

As denoted in the curves, the AH biochar shows a similar behavior to the commercial activated carbon regarding the adsorption of those 2 triazinic herbicides. For the adsorption of atrazine, the commercial sample can adsorb up to 100% of the total concentration in 35 min, while the AH biochar is able to purify the water from 92% of the herbicides in 60 min. In the case of terbuthylazine, the commercial activated carbon can adsorb up to 99% of the TBA in 1 h, while AH biochar can adsorb up to 93% of this triazinic herbicide at the same time. The AH biochar presents a comparable adsorption capacity for atrazine and terbuthylazine with respect to commercial activated carbon. The calculated adsorption capacity is of 5,92 mg/g for the atrazine and 5,51 mg/mg for the TBA considering the commercial activated carbon, while the adsorption capacity for the AH biochars is attesting around 5,47 mg/g and 5,44 mg/g. This efficiency in water purification from these herbicides can be explained in 2 ways: the interaction between the pollutant and the surface of the activated carbon and the presence of micropores in the carbonaceous system. Literature suggests that the dominant mechanism for the adsorption of atrazine involves π–π dispersive interactions between the graphene layers of the adsorbent and the heterocyclic ring of atrazine [60]. The AH biochar presents the highest carbon content (approximately 89%) among the group of activated carbons investigated, explaining the comparable adsorption capacity for the triazinic herbicides with the commercial activated carbon. The presence of those delocalized π-electrons of the graphene layer, which are responsible for the formation of the interaction between the herbicides and the surface of the activated carbon, is strictly correlated to the carbon content of the activated biochar [61]. Regarding the micropores, it is reported in the literature that the volume of micropores with widths corresponding to about 1.5 times the diameter of the target pollutant controlled the adsorption capacity of the activated carbon [62]. In this specific case, the secondary micropores, the ones with a diameter between 0.8 and 2 nm, are the ones that regulate the adsorption of the atrazine [63]. Other factors that might be considered are the external mass transfer, which is accounted to be the slowest step of the adsorption onto the activated carbon [64] and that the atrazine adsorption process is controlled by intraparticle diffusion with a reasonable contribution from boundary layer diffusion, with the intraparticle diffusion into small micropores which is also found to be another limiting step of the process. However, considering the characterization performed, given that the diameter of the atrazine and the terbuthylazine is 1 nm and that the pore distribution consists of bigger pores are present in great numbers on the surface of the activated biochar, the comparable adsorption capacity of the AH biochar with the commercial one, which also shows similar properties can be reasonably justified.

Those results are in line with the literature analysed [65,66], while the work highlights how to transform a widely available biomass, considering that the world hazelnut production is around 1.2 million tons per year [67], which results in various tons of shells available, into an added-value product such as an activated biochar. The production of the biochars permits a new purpose for those wastes, and the performance, comparable with the commercial activated carbons, opens a new perspective on the possibility of deploying those activated biochars into the wastewater treatment industry.

4. Conclusions

This study aimed to evaluate the efficiency of activated biochars derived from agricultural waste biomass, specifically hazelnut shells and rice husks, in the removal of triazinic herbicides—atrazine and terbuthylazine—from contaminated water. The production of these activated biochars involved slow pyrolysis at 700 °C followed by physical activation at 850 °C. These findings highlight the significant potential of utilizing activated biochars as effective adsorbents for herbicide remediation in wastewater treatment applications. Among the biochars tested, the hazelnut shell-derived activated biochar (AH) exhibited the highest adsorption capacities for both atrazine and terbuthylazine, demonstrating performance comparable to that of commercial activated carbon. The adsorption mechanisms identified suggest that the high carbon content of the AH biochar, along with its developed microporous structure, facilitates strong interactions with the targeted herbicides. Specifically, the π–π dispersive interactions between the aromatic structures of the biochar and the heterocyclic rings of the triazine compounds were found to play a crucial role in enhancing adsorption efficiency. Furthermore, the presence of secondary micropores, which align with the dimensions of the herbicide molecules, supports the notion that pore structure is a critical factor influencing adsorption dynamics. This is particularly noteworthy given the increasing regulatory pressures regarding the environmental impacts of synthetic herbicides and the need for sustainable, cost-effective remediation strategies.

Therefore, activated biochar produced from agricultural by-products can be considered for wastewater treatment systems as a viable alternative to conventional activated carbon. The utilization of such biochars aligns with the principles of the circular economy, promoting waste valorization and resource efficiency. By transforming abundant agricultural residues into high-value adsorbents, this approach not only addresses pollution but also contributes to sustainable agricultural practices. Future research should focus on scaling up the production of activated biochars and evaluating their long-term performance in real-world wastewater treatment scenarios. Additionally, investigations into the regeneration and reusability of these biochars could further enhance their feasibility as a sustainable solution for herbicide contamination. Future perspective might include the use of these new characterized and optimized biochars towards other similar pesticides. Moreover, this work could be the base for the valorization of other waste biomasses. Moreover, on the analytic side, further studies into the adsorption of those 2 herbicides onto the developed activate biochar could provide more information about the adsorption process. Overall, the findings of this study provide a compelling case for the adoption of activated biochars in the ongoing efforts to mitigate the environmental impacts of agricultural chemicals.

Declaration of Competing Interest

The authors declare that they have no known competing financial interests or personal relationships that could have appeared to influence the work reported in this paper.

Appendix A. Supporting material

Supplementary data associated with this article can be found in the online version at doi:10.1016/j.nxener.2025.100291.

References

[1] Olivier (ESS) Lavagned Ortigue, 'Pesticides use and trade 1990–2021'.
[2] Pesticides Use, Pesticides trade and pesticides indicators (FAO), 2022https://doi.org/10.4060/cc0918en.
[3] Krzysztof Kuśmierek, Lidia Dąbek, Andrzej Świątkowski, The influence of the shape and grain size of commercial activated carbons on their sorption efficiency towards organic water pollutants, Desalin. Water Treat. 321 (2025) 100996, https://doi.org/10.1016/j.dwt.2025.100996.
[4] Richika Ganjoo et al., 'Activated carbon: fundamentals, classification, and properties', in Activated Carbon, ed. Chandrabhan Verma and Mumtaz A. Quraishi, 1st ed. (The Royal Society of Chemistry, 2023), 1–22, ⟨https://doi.org/10.1039/BK9781839169861-00001⟩.
[5] Panagiota Paraskeva, Dimitrios Kalderis, Evan Diamadopoulos, Production of activated carbon from agricultural by-products, J. Chem. Technol. Biotechnol. 83 (5) (2008) 581–592, https://doi.org/10.1002/jctb.1847.

[6] Drought hits rice production in Italy | World Grain', ⟨https://www.world-grain.com/articles/18295-drought-hits-rice-production-in-italy⟩(Accessed January 7, 2024).
[7] 'Rice | USDA foreign agricultural service', ⟨https://fas.usda.gov/data/production/commodity/0422110⟩(Accessed September 10, 2024).
[8] 'Hazelnut production by country 2024', ⟨https://worldpopulationreview.com/country-rankings/hazelnut-production-by-country⟩ (Accessed September 10, 2024).
[9] Jennifer Bethsass, Aaron Colangelo, European Union Bans Atrazine, while the United States negotiates continued use, Int. J. Occup. Environ. Health 12 (3) (2006) 260–267, https://doi.org/10.1179/oeh.2006.12.3.260.
[10] Simón Navarro, et al., Persistence of four S-triazine herbicides in river, sea and groundwater samples exposed to sunlight and darkness under laboratory conditions, Sci. Total Environ. 329 (1–3) (2004) 87–97, https://doi.org/10.1016/j.scitotenv.2004.03.013.
[11] Navarro et al.
[12] P. Bottoni, et al., Terbuthylazine and other triazines in Italian water resources, Microchem. J. 107 (2013) 136–142, https://doi.org/10.1016/j.microc.2012.06.011.
[13] M. Graymore, F. Stagnitti, G. Allinson, Impacts of atrazine in aquatic ecosystems, Environ. Int. 26 (7–8) (2001) 483–495, https://doi.org/10.1016/S0160-4120(01)00031-9.
[14] Silvia Bozzo, et al., Spatial and temporal trend of groundwater contamination from terbuthylazine and desethyl-terbuthylazine in the Lombardy Region (Italy), Environ. Sci.: Process. Impacts 15 (2) (2013) 366–372, https://doi.org/10.1039/C2EM30536D.
[15] Andrea Di Guardo, Enrico Volpi, Antonio Finizio, Analysis of large-scale monitoring data to identify spatial and temporal trend of risk for terbuthylazine and desethyl-terbuthylazine in surface water bodies of Po Plain (Italy), Sci. Total Environ. 740 (2020) 140121, https://doi.org/10.1016/j.scitotenv.2020.140121.
[16] P. Palma, et al., Occurrence and risk assessment of pesticides in a mediterranean basin with strong agricultural pressure (Guadiana Basin: Southern of Portugal), Sci. Total Environ. 794 (2021) 148703, https://doi.org/10.1016/j.scitotenv.2021.148703.
[17] Karsten Nödler, Tobias Licha, Dimitra Voutsa, Twenty years later – atrazine concentrations in selected coastal waters of the mediterranean and the Baltic Sea, Mar. Pollut. Bull. 70 (1–2) (2013) 112–118, https://doi.org/10.1016/j.marpolbul.2013.02.018.
[18] Samuel P. Hansen, Tiffany L. Messer, Aaron R. Mittelstet, Mitigating the risk of atrazine exposure: identifying hot spots and hot times in surface waters across Nebraska, USA, J. Environ. Manag. 250 (2019) 109424, https://doi.org/10.1016/j.jenvman.2019.109424.
[19] Sandra Parra, et al., Photocatalytic degradation of atrazine using suspended and supported TiO_2, Appl. Catal. B: Environ. 51 (2) (2004) 107–116, https://doi.org/10.1016/j.apcatb.2004.01.021.
[20] Javed Ali Khan, et al., Oxidative degradation of atrazine in aqueous solution by UV/H_2O_2/Fe^{2+}, UV//Fe^{2+} and UV//Fe^{2+} processes: a comparative study, Chem. Eng. J. 218 (2013) 376–383, https://doi.org/10.1016/j.cej.2012.12.055.
[21] Xiaoyan Yang, et al., Biodegradation of atrazine by the novel Citricoccus Sp. strain TT3, Ecotoxicol. Environ. Saf. 147 (2018) 144–150, https://doi.org/10.1016/j.ecoenv.2017.08.046.
[22] Andrea Luca Tasca, Monica Puccini, Ashleigh Fletcher, Terbuthylazine and desethylterbuthylazine: recent occurrence, mobility and removal techniques, Chemosphere 202 (2018) 94–104, https://doi.org/10.1016/j.chemosphere.2018.03.091.
[23] Xinhui Wei, et al., Enhanced adsorption of atrazine on a coal-based activated carbon modified with sodium dodecyl benzene sulfonate under microwave heating, J. Taiwan Inst. Chem. Eng. 77 (2017) 257–262, https://doi.org/10.1016/j.jtice.2017.04.004.
[24] Agnieszka Tomczyk, Zofia Sokołowska, Patrycja Boguta, Biomass type effect on biochar surface characteristic and adsorption capacity relative to silver and copper, Fuel 278 (2020) 118168, https://doi.org/10.1016/j.fuel.2020.118168.
[25] Jin-Hyeob Kwak, et al., Biochar properties and lead(II) adsorption capacity depend on feedstock type, pyrolysis temperature, and steam activation, Chemosphere 231 (2019) 393–404, https://doi.org/10.1016/j.chemosphere.2019.05.128.
[26] Fengyue Suo, et al., Rapid removal of triazine pesticides by P doped biochar and the adsorption mechanism, Chemosphere 235 (2019) 918–925, https://doi.org/10.1016/j.chemosphere.2019.06.158.
[27] Saba Yavari, Amirhossein Malakahmad, Nasiman B. Sapari, Biochar efficiency in pesticides sorption as a function of production variables—a review, Environ. Sci. Pollut. Res. 22 (18) (2015) 13824–13841, https://doi.org/10.1007/s11356-015-5114-2.
[28] Stefanie Kloss, et al., Characterization of slow pyrolysis biochars: effects of feedstocks and pyrolysis temperature on biochar properties, J. Environ. Qual. 41 (4) (2012) 990–1000, https://doi.org/10.2134/jeq2011.0070.
[29] Insha Wani, et al., Effect of pH, volatile content, and pyrolysis conditions on surface area and O/C and H/C ratios of biochar: towards understanding performance of biochar using simplified approach, J. Hazard., Toxic., Radioact. Waste 24 (4) (2020) 04020048, https://doi.org/10.1061/(ASCE)HZ.2153-5515.0000545.
[30] Dilek Angın, Esra Altintig, Tijen Ennil Köse, Influence of process parameters on the surface and chemical properties of activated carbon obtained from biochar by chemical activation, Bioresour. Technol. 148 (2013) 542–549, https://doi.org/10.1016/j.biortech.2013.08.164.
[31] Lilia Longo, et al., Waste biomasses as precursors of catalytic supports in benzaldehyde hydrogenation, Catal. Today 420 (2023) 114038, https://doi.org/10.1016/j.cattod.2023.02.015.
[32] Isabel M. Lima, Akwasi A. Boateng, Kjell T. Klasson, Physicochemical and adsorptive properties of fast-pyrolysis bio-chars and their steam activated counterparts, J. Chem. Technol. Biotechnol. 85 (11) (2010) 1515–1521, https://doi.org/10.1002/jctb.2461.
[33] Melanie Iwanow, et al., Activated carbon as catalyst support: precursors, preparation, modification and characterization, Beilstein J. Org. Chem. 16 (2020) 1188–1202, https://doi.org/10.3762/bjoc.16.104.
[34] Chenxi Zhao, et al., Characteristics evaluation of bio-char produced by pyrolysis from waste hazelnut shell at various temperatures, Energy Sources, Part A: Recovery, Util., Environ. Eff. 21 (2020) 1–11, https://doi.org/10.1080/15567036.2020.1754530.
[35] Yunchao Li, et al., A critical review of the production and advanced utilization of biochar via selective pyrolysis of lignocellulosic biomass, Bioresour. Technol. 312 (2020) 123614, https://doi.org/10.1016/j.biortech.2020.123614.
[36] Suryaprakash Shailendrakumar Shukla, et al., Sustainable use of rice husk for the cleaner production of value-added products, J. Environ. Chem. Eng. 10 (1) (2022) 106899, https://doi.org/10.1016/j.jece.2021.106899.
[37] Md. Masruck Alam, et al., The potentiality of rice husk-derived activated carbon: from synthesis to application, Processes 8 (2) (2020) 203, https://doi.org/10.3390/pr8020203.
[38] Gokalp Gozaydin, Asli Yuksel, Valorization of hazelnut shell waste in hot compressed water, Fuel Process. Technol. 166 (2017) 96–106, https://doi.org/10.1016/j.fuproc.2017.05.034.
[39] Erol Pehlivan, et al., Lead sorption by waste biomass of hazelnut and almond shell, J. Hazard. Mater. 167 (1–3) (2009) 1203–1208, https://doi.org/10.1016/j.jhazmat.2009.01.126.
[40] Mehmet Uğurlu, Ahmet Gürses, Metin Açıkyıldız, Comparison of textile dyeing effluent adsorption on commercial activated carbon and activated carbon prepared from olive stone by $ZnCl_2$ activation, Microporous Mesoporous Mater. 111 (1–3) (April 2008) 228–235, https://doi.org/10.1016/j.micromeso.2007.07.034.
[41] Shi-Xiang Zhao, Na Ta, Xu-Dong Wang, Effect of temperature on the structural and physicochemical properties of biochar with apple tree branches as feedstock material, Energies 10 (9) (2017) 1293, https://doi.org/10.3390/en10091293.
[42] Bareen Bushra, Neelancherry Remya, Biochar from pyrolysis of rice husk biomass—characteristics, modification and environmental application, Biomass Convers. Biorefinery 14 (2024) 5759–5770, https://doi.org/10.1007/s13399-020-01092-3.
[43] Menegazzo Federica, et al., On the applications as catalytic support of biochars obtained by pyrolysis of waste biomasses, Chem. Eng. Trans. 109 (2024) 367–372, https://doi.org/10.3303/CET24109062.
[44] Somayeh Taghavi, et al., Activated biochars as sustainable and effective supports for hydrogenations, Carbon Trends 13 (2023) 100316, https://doi.org/10.1016/j.cartre.2023.100316.
[45] M.D. Donohue, G.L. Aranovich, Classification of Gibbs adsorption isotherms, Adv. Colloid Interface Sci. 76-77 (1998) 137–152, https://doi.org/10.1016/S0001-8686(98)00044-X.
[46] Pelin Ozpinar, et al., Activated carbons prepared from hazelnut shell waste by phosphoric acid activation for supercapacitor electrode applications and comprehensive electrochemical analysis, Renew. Energy 189 (2022) 535–548, https://doi.org/10.1016/j.renene.2022.02.126.
[47] Peng Fu, et al., FTIR study of pyrolysis products evolving from typical agricultural residues, J. Anal. Appl. Pyrolysis 88 (2) (2010) 117–123, https://doi.org/10.1016/j.jaap.2010.03.004.
[48] Li Zhang, et al., Synthesis and characterization of different activated biochar catalysts for removal of biomass pyrolysis tar, Energy 232 (2021) 120927, https://doi.org/10.1016/j.energy.2021.120927.
[49] Tzong-Horng Liou, et al., Sustainable utilization of rice husk waste for preparation of ordered nanostructured mesoporous silica and mesoporous carbon: characterization and adsorption performance, Colloids Surf. A: Physicochem. Eng. Asp. 636 (2022) 128150, https://doi.org/10.1016/j.colsurfa.2021.128150.
[50] J.L. Figueiredo, et al., Modification of the surface chemistry of activated carbons, Carbon 37 (9) (1999) 1379–1389, https://doi.org/10.1016/S0008-6223(98)00333-9.
[51] Takafumi Ishii, Takashi Kyotani, Temperature Programmed Desorption, in: Michio Inagaki, Feiyu Kang (Eds.), Materials Science and Engineering of Carbon, Elsevier, Cambridge, MA, 2016, pp. 287–305, https://doi.org/10.1016/B978-0-12-805256-3.00014-3.
[52] Brenda R. Baillie, Herbicide concentrations in waterways following aerial application in a steepland planted forest in New Zealand, N. Z. J. For. Sci. 46 (1) (2016) 16, https://doi.org/10.1186/s40490-016-0072-0.
[53] Albrecht Paschke, et al., Octanol/water partition coefficient of selected herbicides: determination using shake-flask method and reversed-phase high-performance liquid chromatography, J. Chem. Eng. Data 49 (6) (2004) 1639–1642, https://doi.org/10.1021/je049947x.
[54] Nathalie Bonvallot, Paul Harrison, Miranda Loh, 'Trichloroethylene', in WHO Guidelines for Indoor Air Quality: Selected Pollutants, World Health Organization, Geneva, 2010⟨https://www.ncbi.nlm.nih.gov/books/NBK138713/⟩.
[55] Iwona Lupul, et al., Adsorption of atrazine on hemp stem-based activated carbons with different surface chemistry, Adsorption 21 (6–7) (2015) 489–498, https://doi.org/10.1007/s10450-015-9689-1.
[56] A. Erto, et al., Experimental and statistical analysis of trichloroethylene adsorption onto activated carbon, Chem. Eng. J. 156 (2) (2010) 353–359, https://doi.org/10.1016/j.cej.2009.10.034.
[57] Muniandy Gayathiri, et al., Activated carbon from biomass waste precursors: factors affecting production and adsorption mechanism, Chemosphere 294 (2022) 133764, https://doi.org/10.1016/j.chemosphere.2022.133764.

[58] Lima, Boateng, and Klasson, Physicochemical and adsorptive properties of fast-pyrolysis bio-chars and their steam activated counterparts.
[59] Atrazine and its metabolites in drinking-water-background document for development of WHO Guidelines for Drinking-Water Quality (2009).
[60] Feng Xiao, Joseph J. Pignatello, Interactions of triazine herbicides with biochar: steric and electronic effects, Water Res. 80 (2015) 179–188, https://doi.org/10.1016/j.watres.2015.04.040.
[61] Carlos Moreno-Castilla, Adsorption of organic molecules from aqueous solutions on carbon materials, Carbon 42 (1) (2004) 83–94, https://doi.org/10.1016/j.carbon.2003.09.022.
[62] Patricia A. Quinlivan, Lei Li, Detlef R.U. Knappe, Effects of activated carbon characteristics on the simultaneous adsorption of aqueous organic micropollutants and natural organic matter, Water Res. 39 (8) (2005) 1663–1673, https://doi.org/10.1016/j.watres.2005.01.029.
[63] Costas Pelekani, Vernon L. Snoeyink, Competitive adsorption between atrazine and methylene blue on activated carbon: the importance of pore size distribution, Carbon 38 (10) (2000) 1423–1436, https://doi.org/10.1016/S0008-6223(99)00261-4.
[64] P. Chingombe, B. Saha, R.J. Wakeman, Sorption of atrazine on conventional and surface modified activated carbons, J. Colloid Interface Sci. 302 (2) (2006) 408–416, https://doi.org/10.1016/j.jcis.2006.06.065.
[65] Xuchen Zhao, et al., Properties comparison of biochars from corn straw with different pretreatment and sorption behaviour of atrazine, Bioresour. Technol. 147 (2013) 338–344, https://doi.org/10.1016/j.biortech.2013.08.042.
[66] Cleuciane Tillvitz Do Nascimento, et al., Adsorption of atrazine from aqueous systems on chemically activated biochar produced from corn straw, J. Environ. Chem. Eng. 10 (1) (2022) 107039, https://doi.org/10.1016/j.jece.2021.107039.
[67] 'FAOSTAT', ⟨https://www.fao.org/faostat/en/#data/QCL⟩. (Accessed November 18, 2024).